Effective Hamiltonian for surface states of topological insulator thin films with hexagonal warping

Zhuo Bin Siu, Seng Ghee Tan, and Mansoor B. A. Jalil

Citation: AIP Advances **6**, 055706 (2016); doi: 10.1063/1.4943416
View online: http://dx.doi.org/10.1063/1.4943416
View Table of Contents: http://scitation.aip.org/content/aip/journal/adva/6/5?ver=pdfcov
Published by the AIP Publishing

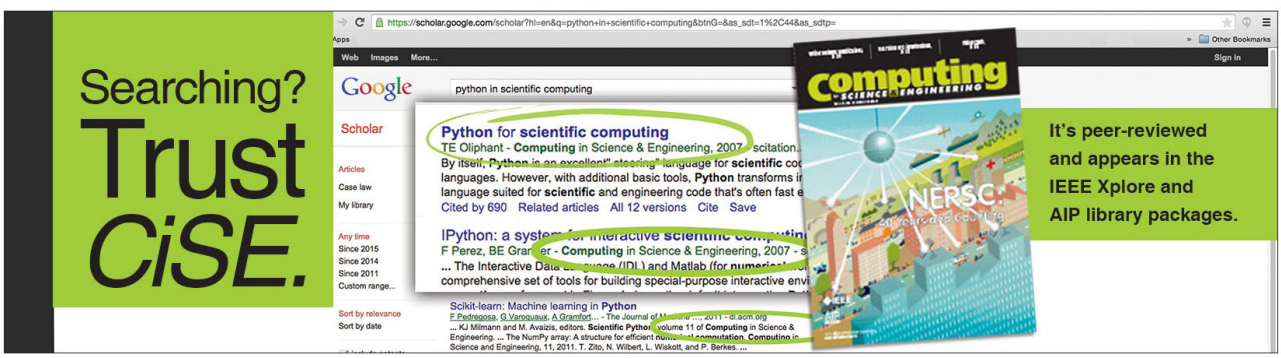

Effective Hamiltonian for surface states of topological insulator thin films with hexagonal warping

Zhuo Bin Siu,[1] Seng Ghee Tan,[2] and Mansoor B. A. Jalil[1]
[1]*Computational Nanoelectronics and Nanodevices Laboratory, Electrical and Computer Engineering Department, National University of Singapore, Singapore*
[2]*Data Storage Institute, Agency for Science, Technology and Research (A*STAR), Singapore*

(Presented 15 January 2016; received 5 November 2015; accepted 22 December 2015; published online 10 March 2016)

The effective Hamiltonian of the surface states on semi-infinite slabs of the topological insulators (TI) Bi_2Te_3 and Bi_2Se_3 require the addition of a cubic momentum hexagonal warping term on top of the usual Dirac fermion Hamiltonian in order to reproduce the experimentally measured constant energy contours at intermediate values of Fermi energy. In this work, we derive the effective Hamiltonian for the surface states of a Bi_2Se_3 thin film incorporating the corresponding hexagonal warping terms. We then calculate the dispersion relation of the effective Hamiltonian and show that the hexagonal warping leads distorts the equal energy contours from the circular cross sections of the Dirac cones. [http://dx.doi.org/10.1063/1.4943416]

I. INTRODUCTION

Experimental measurements[1,2] of the Fermi surfaces of the surface states on semi-infinite slabs of the three-dimensional topological insulator (TI) Bi_2Te_3 reveal deviations at moderate Fermi energies from the circular cross sections of the Dirac cones predicted by the Dirac fermion Hamiltonian $H = v(\vec{p} \times \hat{z}) \cdot \vec{\sigma}$. This discrepancy led Fu to introduce a hexagonal warping term to the Dirac Hamiltonian based on the symmetries of the underlying crystal structure in order to reproduce the experimental results.[3] The effective Hamiltonian now reads

$$H = v(\vec{p} \times \hat{z}) \cdot \vec{\sigma} + \lambda \sigma_z (k_x^3 - 3k_x k_y^2) \tag{1}$$

where the quintuple layers are on the xy plane. A hexagonal warping in the surface states of Bi_2Se_3 which can also be described by Eq. (1) was experimentally discovered a year later.[4]

We showed in an earlier work[5] that the additional hexagonal warping term in a semi-infinite Bi_2Te_3 slab leads to the distortion of the Fermi surface and the opening of a bandgap by an *in-plane* magnetization, both of which would not have occurred in the absence of the hexagonal warping term.

In this work, we derive the effective Hamiltonian for the surface states of a TI thin film[6–8] of small, finite thickness, and infinite width and length which incorporates the hexagonal warping. A key feature that distinguishes a TI thin film from a TI slab of semi-infinite thickness is that there are now two surfaces, which we label as the top and bottom surfaces. Each of these surfaces admits states localized at the respective surfaces. The states localized on the top and bottom surfaces are not independent of each other but are correlated, for example by the boundary condition that their wavefunctions have to simultaneously vanish at both surfaces. The coupling between the localized states on the two surfaces leads to additional effects absent in semi-infinite slabs where only one surface is present.

II. FOUR-BAND HAMILTONIAN

We start from the effective four-band model Hamiltonian of Liu *et al.*[9] which describes both the bulk and surface states of the BiSe family of topological insulators

$$H_{(4B)} = (C_0 + C_1k_z^2 + C_2k_\parallel^2)\mathbb{I}_4 + (M_0 + M_1k_z^2 + M_2k_\parallel^2)\Gamma_5 + B\Gamma_4k_z + A(\Gamma_1k_y - \Gamma_2k_x) + R_1\Gamma_3(k_x^3 - 3k_xk_y^2) + R_2\Gamma_4(3k_x^2k_y - k_y^3) \quad (2)$$

where $\Gamma_1 = \sigma_x \otimes t_1, \Gamma_2 = \sigma_y \otimes t_1, \Gamma_3 = \sigma_z \otimes t_1, \Gamma_4 = \mathbb{I}_\sigma \otimes t_2$ and $\Gamma_5 = \mathbb{I}_\sigma \otimes t_3$, and $k_\parallel^2 \equiv k_x^2 + k_y^2$. (The subscript $(4B)$ indicates that this is a four band Hamiltonian.) The t's can be interpreted as describing the orbital degree of freedom and the σ's the real spins. Fu's hexagonal warping term in Eq. (1) can be derived from Eq. (2) and originate from the R_1 and R_2 terms.

Following Lu *et al.*,[8] we divide Eq. (2) into a 'perpendicular Hamiltonian' $H_{(4B),\perp}$ containing constant terms and derivatives perpendicular to the two surfaces but excluding the R_1 and R_2 terms, and a 'parallel Hamiltonian' $H_{(4B),\parallel}$ containing the remaining terms. We solve for the eigenstates of the perpendicular Hamiltonian localized at the two film surfaces, and treat the $H_{(4B),\parallel}$ as a perturbation to $H_{(4B),\perp}$. The localized eigenstates of $H_{(4B),\perp}$ are at least two-fold degenerate due to the spin degeneracy. Consistent with standard degenerate perturbation theory, the effective Hamiltonian for the surface states is then obtained obtained by projecting $H_{(4B),\parallel}$ onto the basis of the localized eigenstates of $H_{(4B),\perp}$.

III. EFFECTIVE HAMILTONIAN

We consider a thin film with normal parallel to the z crystal growth direction. Accordingly, the corresponding $H_{(4B),\perp}$ containing constant terms and the z derivatives reads

$$H_{(4B),\perp} = \mathbb{I}_\sigma\big((C_0 + C_1k_z^2)\mathbb{I}_t + (M_0 + M_1k_z^2)t_z + B_0k_zt_y\big). \quad (3)$$

As $H_{(4B),\perp}$ is diagonal in spin, we can consider the spin up and spin down states separately. We look for states localized at the surface boundaries with the form of $\exp(\lambda z)$, so that $k_z \to -i\lambda$. For a given energy E_f, diagonalizing Eq. (3) and equating the eigenenergies with E_f gives

$$\lambda_\pm^2 = -\frac{1}{2(C_1^2 - M_1^2)}\Big(B_0^2 - 2C_0C_1 + 2C_1E_f + 2M_0M_1 \pm \big(B_0^4 + 4(C_1M_0 - C_0M_1 + E_fM_1)^2 + B_0^2(-4C_0C_1 + 4C_1E_f + 4M_0M_1)\big)^{\frac{1}{2}}\Big). \quad (4)$$

This gives two values of λ^2, whose square roots we denote as $\lambda_\pm$. We seek linear combinations of these exponentials which disappear simultaneously at the two surfaces at $z = \pm W/2$ where W is the thickness of the film. Two such combinations are

$$f_+ \equiv \frac{\cosh(\lambda_+z)}{\cosh(\lambda_+W/2)} - \frac{\cosh(\lambda_-z)}{\cosh(\lambda_-W/2)},$$
$$f_- \equiv \frac{\sinh(\lambda_+z)}{\sinh(\lambda_+W/2)} - \frac{\sinh(\lambda_-z)}{\sinh(\lambda_-W/2)}.$$

Using the ansatz that the spin up eigenstates are in the form of

$$\chi^\uparrow \equiv \begin{pmatrix} f_+ \\ c_-f_- \end{pmatrix}, \varphi^\uparrow \equiv \begin{pmatrix} f_- \\ c_+f_+ \end{pmatrix} \quad (5)$$

and putting, for example, $\chi^\uparrow$ into $(H - E_f)\chi^\uparrow = 0$ gives a set of 2 equations which contain hyperbolic trigonometric functions of z, but which should nonetheless give 0 everywhere independent of the value of z. This indicates that the coefficients in front of the various hyperbolic trigonometric functions should vanish. The coefficients of $\cosh(\lambda_+z)$ and $\cosh(\lambda_-z)$ in the upper and lower components of $(H - E_f)\chi^\uparrow = 0$ respectively yield two different equations for c_-. Imposing the condition that these two equations for c_- agree with each other gives

$$\frac{(C_0 - E_f + M_0 - (C_1 + M_1)\lambda_+^2)\lambda_- \tanh(W\lambda_+/2)}{(C_0 - E_f + M_0 - (C_1 + M_1)\lambda_-^2)\lambda_+ \tanh(W\lambda_-/2)} = 1. \quad (6)$$

This is a transcendental equation in E_f due to the $\lambda_\pm$ dependence on E_f via Eq. (4), which can be solved numerically. Once we find an energy where the values of c_- calculated from the

equations resulting coefficients of $\cosh(\lambda_{\pm\lambda} z)$ agree, we can use either expression to obtain the value of c_-. Applying a similar procedure on $(H - E_f)\varphi^{\uparrow} = 0$ with $\varphi^{\uparrow}$ as defined in Eq. (5) gives a corresponding equation to Eq. (6) for the φ states which can be solved numerically to give E_φ and its corresponding eigenspinor. The Hamiltonian for the spin down states is identical to the one for spin up states. The spin down eigenstates and eigenenergies are thus given by the same equations as the spin up states.

Now projecting $H_{(4B),\parallel}$ into the basis of $(\chi^{\uparrow/\downarrow}, \varphi^{\uparrow/\downarrow})$ and introducing the shorthand $C_i \equiv \int \mathrm{d}z\, \langle \chi^{\uparrow}|t_i|\chi^{\uparrow}\rangle$, $P_i \equiv \int \mathrm{d}z\, \langle \chi^{\uparrow}|t_i|\chi^{\uparrow}\rangle$ and $M_i \equiv \int \mathrm{d}z\, \langle \chi^{\uparrow}|t_i|\phi^{\uparrow}\rangle$ ('C' for χ, 'P' for φ, and 'M' for 'mixed'), we have, using $\int \mathrm{d}z\, f_+ f_- = 0$,

$$\begin{aligned} H_{(2B)} = {} & \frac{1}{2}\left((E_\varphi + E_\chi)\mathbb{I}_4 + (E_\varphi - E_\chi)\tilde{\tau}_z\mathbb{I}_\sigma\right) + k_\parallel^2\Big(C_2\mathbb{I}_4 + \frac{M_2}{2}\big((C_z + P_z)\mathbb{I}_4 + (C_z - P_z)\mathbb{I}_\sigma\tau_z\big) \\ & + A_0(\mathrm{Re}(M_x)\tilde{\tau}_x - \mathrm{Im}(M_x)\tilde{\tau}_y)(k_y\sigma_x - k_x\sigma_y) \\ & + (\mathrm{Re}(M_x)\tilde{\tau}_x - \mathrm{Im}(M_x)\tilde{\tau}_y)(R_1(k_x^3 - 3k_xk_y^2)\sigma_z + R_2(3k_x^2k_y - k_y^3)\mathbb{I}_\sigma) \end{aligned} \tag{7}$$

In Eq. (7), the $\tilde{\tau}$'s can be interpreted as a degree of freedom indicative of the relative parities of the real and imaginary parts of the wavefunction. In particular, an examination of the eigenstates $\tilde{\tau}$ polarized along the $\pm\tilde{\tau}_i$, $(i = x, y, z)$, directions indicates that the $\tilde{\tau}_x$ polarization is indicative of whether the states are localized near the top or bottom surface of the film.

In what follows, we use the material parameters for Bi_2Se_3 from Ref. 9 for all the parameters in Eq. (2) except for R_1 and R_2 in our numerical calculations. Although the hexagonal warping in Bi_2Te_3 is stronger than in Bi_2Se_3, the only set of numerical values for the material parameters in Eq. (2) available in published literature which we are aware of for Bi_2Te_3 is in Ref. 9. This set of parameters does not admit a solution for real E_f in Eq. (6), and hence does not support the existence of localized surface states. This contradicts experimental ARPES observations of localized surface states[10,11] in Bi_2Te_3 thin films, and casts doubts on the validity of modeling Bi_2Te_3 thin films with Eq. (2) and the set of parameters in Ref. 9. We therefore eschew Bi_2Te_3 in favor of Bi_2Se_3 where the available numerical parameters allow us to make predictions closer to actual experimental results. Deriving the effective Hamiltonian for a semi-infinite slab, we find that A_0 and R_1 in Eq. (2) correspond to v and λ respectively in Eq. (1). The value of A_0 obtained from first-principles calculations in Ref. 9 for Bi_2Se_3 matches the experimentally determined value in Ref. 4 within 10%, but the value of R_1 is smaller than λ by a factor of 2.5. Accordingly we scale the values of R_1 and R_2 from Ref. 9 up by a factor of 2.5 in our calculations.

Using this set of parameters, we find numerically that M_x is real for all values of thicknesses at which surface states exist. Dropping 0 terms and performing a rotation of the $\tilde{\tau}$ axis, $\tilde{\tau} \to \tau$, so that the τ_z polarization now indicates which surface the states are localized at, the effective Hamiltonian takes the form of

$$\begin{aligned} H = {} & E_0\mathbb{I}_4 - E_\delta\tau_x\mathbb{I}_\sigma + (-\mu\mathbb{I}_4 + \mu'\tau_x\mathbb{I}_\sigma)k_\parallel^2 + v\tau_z(k_y\sigma_x - k_x\sigma_y) \\ & + \tau_z(h_1(k_x^3 - 3k_xk_y^2)\sigma_z - h_2(3k_x^2k_y - k_y^3)\mathbb{I}_\sigma) \end{aligned} \tag{8}$$

where the explicit form of the parameters that appear above can be read off in comparison with Eq. (7). We have introduced - signs in front of some of the terms so that the parameters assume positive values within the thickness ranges considered.

Recalling that the τ_z polarization is associated with whether the state is localized nearer the top or bottom surface of the film, the second line of Eq. (8) is the familiar result that the surface states on each of the two surfaces of a TI film are described by the usual Dirac fermion Hamiltonian $v(\vec{k} \times \vec{\sigma}) \cdot \hat{n}$ where $\hat{n}$ has opposite signs on the two surfaces. The terms proportional to τ_x in the first line denote the coupling between the two surfaces of the film. The last line in Eq. (8) represents the hexagonal warping. The first term $h_1\tau_z(k_x^3 - 3k_xk_y^2)\sigma_z$ on the last line has the familiar form of the hexagonal warping on a semi-infinite slab (the term proportional to λ in Eq. (1)) with an additional factor of τ_z denoting that this term has opposite signs on the two surfaces. The second term $h_2(3k_x^2k_y - k_y^3)\tau_z\mathbb{I}_\sigma$ is 0 on the semi-infinite slab as the corresponding expression for h_2 on a semi-infinite geometry is proportional to expectation values of terms which evaluate to 0. h_2 is however finite on the thin film geometry, and leads to an additional shift in energy cubic in momentum.

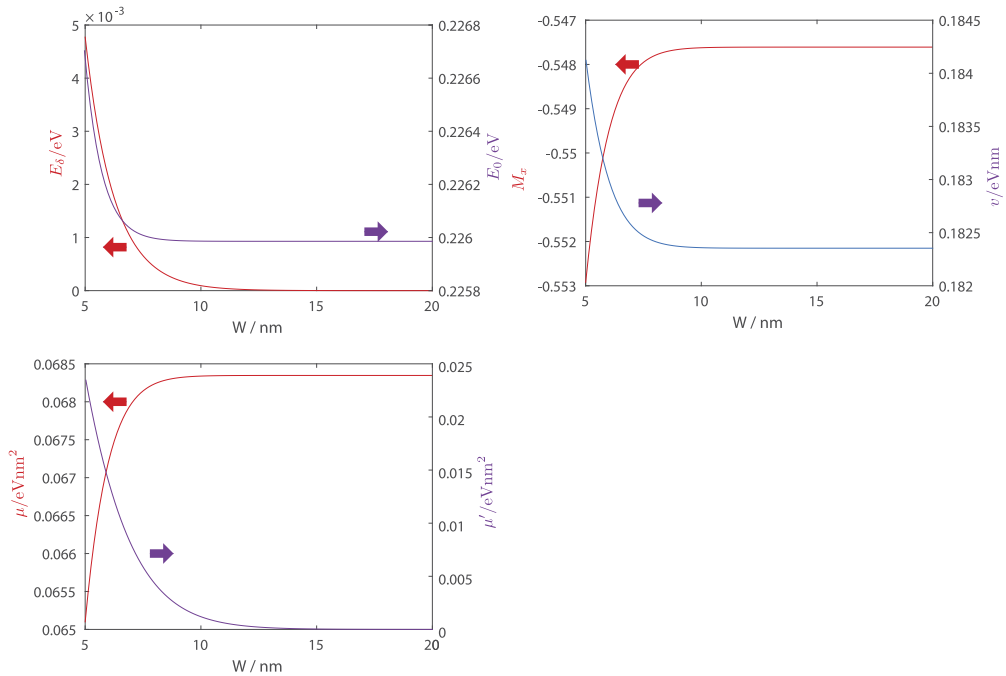

FIG. 1. The values of M_x, and the other parameters not proportional to M_x in Eq. (8) as a function of the film thickness.

Fig. 1 shows the computed values of M_x, which h_1, h_2 and v are directly proportional to, and the other parameters in Eq. (8) as a function of the film thickness from 5 nm to 15 nm. (The $|\chi\rangle$ states emerge at 0.76 nm and the $|\varphi\rangle$ states at 3.94 nm. We need both types of surface states to exist in order to construct the effective Hamiltonian.) The parameters undergo relatively large changes at small thicknesses and approximately attain their asymptotic values in the limit of infinite thickness at around 15 nm. (The value of E_0 is shifted with respect to the Dirac energy of semi-infinite thick slabs of -0.3 eV[12] due to the finite thickness.) Except for μ' and E_δ the magnitudes of the remaining parameters do not change by more than 1% in the thickness range plotted.

IV. EIGENSTATES OF EFFECTIVE HAMILTONIAN

We now exhibit some properties of the eigenstates of Eq. (8) by computing its dispersion relations numerically.

Panels (a) and (b) of Fig. 2 show the dispersion relations for a 5 nm thick film and a 15 nm thick film respectively. These two thicknesses represent the two extremes of a thin film not much thicker than the minimum thickness needed to support the formation of localized surface states, and a thicker film at which the effective Hamiltonian parameters are almost at their infinite thickness asymptotic values. The biggest difference between the two thicknesses is that a bandgap at $\vec{k} = 0$ is present at the smaller thickness and absent at the larger one. This difference is due to the decrease of E_δ from a finite value to 0 with increasing thickness. The increase of E_0 with thickness gives a slight upwards shift in the dispersion relations along the energy axis at different thicknesses. Since the dispersion relations at different thicknesses are otherwise qualitatively similar, we shall concentrate on the 15 nm thick film.

Compare now the cases where the hexagonal warping is present in the solid curves of panel (b) and switched off in the dotted curves. The hexagonal warping leads to an energy splitting of the otherwise two-fold degenerate bands. (The splitting is larger in thinner films.) Comparing between panels (c) and (d) of the figure, it is evident that the splitting occurs with different magnitudes along different directions in k-space. Panel (d) shows that this anisotropic splitting leads to a deviation of the equal energy contours from the circular cross section of the two overlapping Dirac cones to a

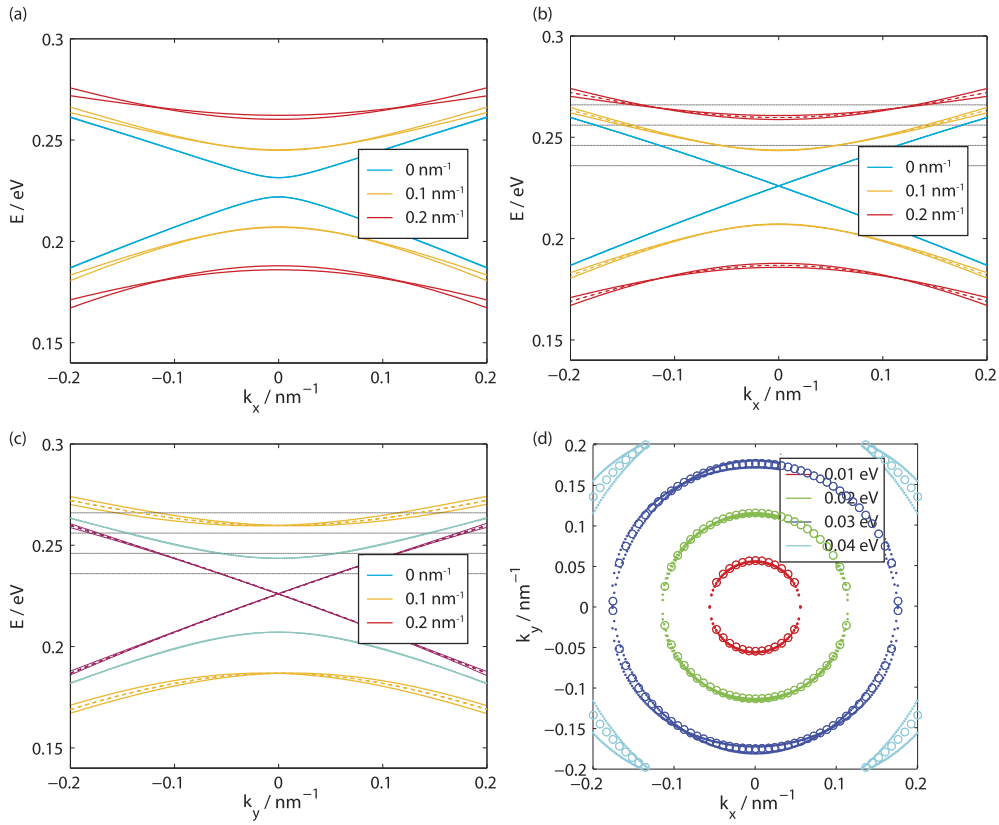

FIG. 2. (a) The dispersion relation for a 5 nm thick Bi_2Se_3 film as a function of k_x for various values of k_y labeled in the legend. (b) The solid lines indicate the dispersion relations for a 15 nm thick Bi_2Se_3 film as a function of k_x for various values of k_y. The thin dotted lines indicate the dispersion relations calculated with the hexagonal warping terms h_1 and h_2 set to 0. (c) The dispersion relations for a 15 nm thick film as a function of k_y for various values of k_x with (solid lines) and without (dotted lines) the hexagonal warping terms. (d) The equal energy contours in k-space for a 15 nm thick film at various values of energy with (solid circles) and without (hollow circles) hexagonal warping. The values in the legend indicate the energy of each curve as an offset from E_0. These values of energy are denoted by the horizontal dotted lines in panels (b) and (c) of the figure.

profile which exhibits a six-fold rotational symmetry. This six-fold symmetry is a hallmark of the hexagonal warping and is reminiscent of that experimentally observed in semi-infinite bulk slabs of Bi_2Te_3 and Bi_2Se_3.

We finally consider the effects of applying an in-plane magnetization in the y direction modeled by the addition of a $m_y\mathbb{I}_\tau\sigma_y$ term to the Hamiltonian Eq. (8).

Fig. 3 shows the dispersion relations and constant energy contours for a 15 nm thick film for $m_y = 0.005$ eV. There is a significant difference between the effects of the magnetization in the thin film, and in a semi-infinite slab. In the latter, the hexagonal warping allows an *in-plane* magnetization opens up a bandgap.[5] In contrast, panel (a) shows that for a thin film there is no bandgap opening. Instead the coupling between the spin σ and surface τ degrees of freedom here leads causes the in-plane magnetization to generate a k space separation between the two initially overlapping Dirac cones centered at $\vec{k} = 0$. Comparing between the dispersion relations of panel (a) where the hexagonal warping is present (solid lines) and switched off (dashed lines), we see that the hexagonal warping shifts the band bottom of the $E - k_x$ curves at a given finite value of k_y away from $k_x = 0$. This shift occurs in opposite directions for the hole and particle bands, and distorts the constant energy contours away from the perfect circles of the Dirac cones. The distortion in the presence of an in-plane magnetization due to hexagonal warping has also been reported in semi-infinite Bi_2Te_3 slabs.[5]

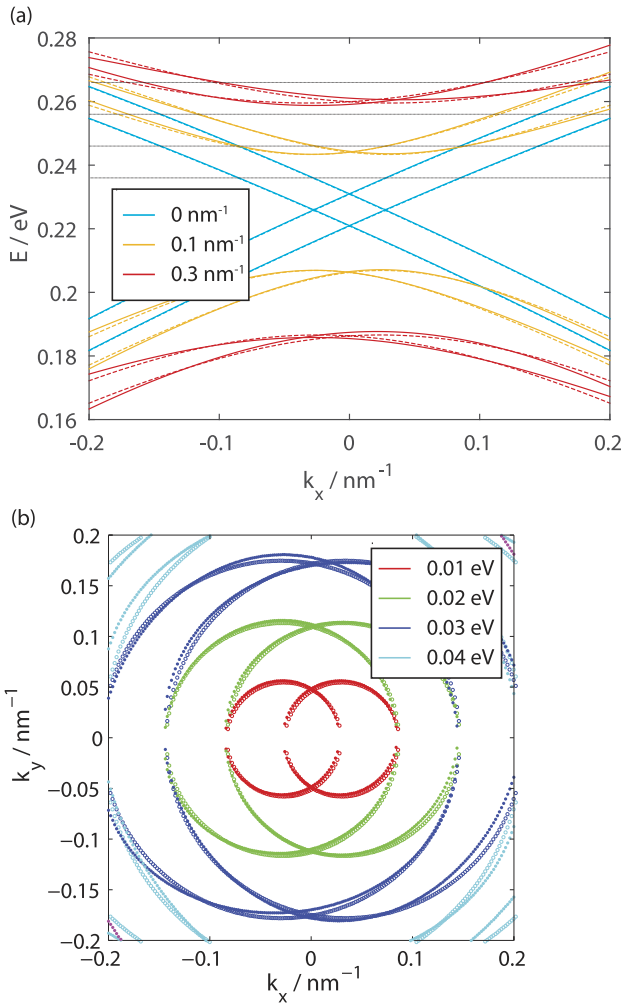

FIG. 3. (a) The dispersion relation for a 15 nm thick film as a function of k_x for various values of k_y in the presence of a magnetization corresponding to a Zeeman splitting $m_y = 0.005$ eV. The solid lines indicate the dispersion relations for the film with hexagonal warping, and the dotted lines indicate the dispersion relations with $h_1 = h_2 = 0$. (b) The equal energy contours in k-space for a 15nm thick film at various values of energy labeled by the displacement of the energy away from E_0 in the legend and corresponding thin dotted lines in panel (a) of the figure.

V. CONCLUSION

In this work, we derived an effective Hamiltonian for the surface states of a topological insulator thin film incorporating the hexagonal warping terms and computed the numerical values of parameters within. We then calculated the eigenstates of the effective Hamiltonian at two representative thicknesses, and showed that the hexagonal warping leads to a lifting of the energy degeneracy of the energy bands as well as a six-fold symmetric distortion of the constant energy contours away from the usual circular cross sections of Dirac cones. In particular, the thin film with hexagonal warping differs from a semi-infinite thick TI slab in that whereas an in-plane magnetization opens up a bandgap in the latter, it does not in the former.

ACKNOWLEDGMENTS

We thank the MOE Tier II grant MOE2013-T2-2-125 (NUS Grant No. R-263-000-B10-112), and the National Research Foundation of Singapore under the CRP Program "Next Generation Spin

Torque Memories: From Fundamental Physics to Applications" NRF-CRP12-2013-01 for financial support.

[1] D. Hsieh *et al.*, Nature **460**, 1101 (2009).
[2] Y. L. Chen *et al.*, Science **325**, 178 (2009).
[3] L. Fu, Phy. Rev. Lett. **103**, 266801 (2009).
[4] K. Kuroda *et al.*, Phys. Rev. Lett. **105**, 076802 (2010).
[5] Z. B. Siu, M. B. A. Jalil, and S. G. Tan, Sci. Rep. **4**, 5062 (2014).
[6] J. Linder, T. Yokoyama, and A. Sudbø, Phys. Rev. B **80**, 205401 (2009).
[7] C.-X. Liu *et al.*, Phys. Rev. B **81**, 041307 (2010).
[8] H.-Z. Lu *et al.*, Phys. Rev. B **81**, 115407 (2010).
[9] C.-X. Liu *et al.*, Phys. Rev. B **82**, 045122 (2010).
[10] L. Plucinski *et al.*, Appl. Phys. Lett. **98**, 222503 (2011).
[11] X. Chen *et al.*, Adv. Mater. **22**, 4002 (2010).
[12] Y. Xia *et al.*, Nature Phys. **5**, 398 (2009).